Journal of Materials Chemistry A

Intercalating cobalt cation to Co_9S_8 interlayer for highly efficient and stable electrocatalytic hydrogen evolution

Journal:	*Journal of Materials Chemistry A*
Manuscript ID	TA-ART-11-2021-009755.R1
Article Type:	Paper
Date Submitted by the Author:	21-Dec-2021
Complete List of Authors:	Tian, Bin; Jackson State University, Department of Chemistry, Physics and Atmospheric Science Kolodziejczyk, Wojciech; Jackson State University, Department of Chemistry, Physics and Atmospheric Science Saloni, Julia; Jackson State University, Interdisciplinary Center for Nanotoxicity, Department of Chemistry, Physics and Atmospheric Sciences CHEAH, POHLEE; Jackson State University, Department of Chemistry, Physics and Atmospheric Science Qu, Jing; Jackson State University, Department of Chemistry, Physics and Atmospheric Science Han, Fengxiang; Jackson State University, Department of Chemistry, Physics and Atmospheric Science Cao, Dongmei; Louisiana State University, Material Characterization Center Zhu, Xianchun; Jackson State University, Department of Chemistry, Physics and Atmospheric Science Zhao, Yongfeng; Jackson State University, Department of Chemistry, Physics and Atmospheric Science

Intercalating cobalt cation to Co_9S_8 interlayer for highly efficient and stable electrocatalytic hydrogen evolution

Bin Tian[a], Wojciech Kolodziejczyk[a], Julia Saloni[a], Pohlee Cheah[a], Jing Qu[a], Fengxiang Han[a], Dongmei Cao[b], Xianchun Zhu[a], Yongfeng Zhao[a,]*

[a]Department of Chemistry, Physics and Atmospheric Science, Jackson State University, Jackson, MS 39217, USA

[b]Material Characterization Center, Louisiana State University, Baton Rouge, LA 70803, USA

Abstract

Non-noble metal based electrocatalysts for hydrogen evolution reactions hold great potential for commercial applications. However, effective design strategies are highly needed to manipulate the catalyst structures for high activity and stability comparable to those of noble-metal based electrocatalysts. Herein, we present a facile route to synthesize Co^{2+} intercalated Co_9S_8 layered electrocatalysts (Co^{2+}-Co_9S_8) (the layer distance up to 1.08 nm) via a one-step solvothermal method. Benefiting from a large layer distance and efficient electron transfer between layers, the Co^{2+}-Co_9S_8 hybrid shows outstanding electrocatalytic hydrogen evolution performance in an acid electrolyte. The electrocatalytic performance is even better than that of 20 % Pt/C at <-0.54 V region with an overpotential of 86 mV at a current density of 10 mA cm^{-2} in 0.5 mol L^{-1} H_2SO_4. More importantly, the system can maintain excellent stability for more than 12 h without obvious decay. This study not only presents a novel and efficient approach to synthesize Co cations intercalated cobalt sulfide for stable electrocatalytic hydrogen evolution reaction but also provides an avenue for the design of intercalated materials used in other energy applications.

Keywords: Electrocatalyst · 2D materials · Hydrogen evolution reaction · Intercalated Co_9S_8

Introduction

Since the first industrial revolution, the utilization of fossil fuels has brought great convenience to modern society but also results in serious environmental problems.[1-3] Especially with the depletion of fossil fuels, it is urgent to construct a new energy system.[4] Solar energy is considered as an endless and green energy source. It will be an ideal energy system if we can convert solar energy into chemical fuels, which can then be stored and utilized. One of the promising ways is the formation of hydrogen (H_2) through highly efficient and sustainable electrolysis of water owing to the abundant water sources on earth.[5, 6] So far, noble metal-based (Pt, Ir, Rh, etc.) materials show promising catalytic activities; however, rare reserves and exorbitant prices limit their wide range of commercial applications.[7] The long-term stability of these precious metal catalysts is hardly satisfactory, especially in an acid electrolyte.[8]

In the past few decades, great efforts have been devoted to the development of non-noble metal-based catalysts for hydrogen evolution reaction (HER). Particularly, earth-abundant transition metal chalcogenides (TMCs), such as MoS_2, Co_9S_8, FeS_2, etc., have been demonstrated as promising catalytic materials for HER inspired by the structure/composition of nitrogenase and hydrogenase.[9-12] But their activity is far from satisfactory compared with that of Pt-based catalysts due to low conductivity.[13] In addition, TMCs suffer from serious stability problems because of the dissolution or agglomeration during the reaction.[14] There have been reports that carbon materials, such as carbon nanotubes, graphene, and carbon dots, can accelerate the electron transfer to the active sites as well as stabilize the structure of catalysts.[15] Nevertheless,

the performance reported to date is still unsatisfying, partially due to the lack of an efficient structure control for fully utilizing active sites of the catalysts.

Recently, 2D materials, especially those with an ultrathin 2D structure, have attracted considerable attention because their excellent physical, chemical, electronic, and optical properties not only make them promising for technological applications but also provide opportunities to discover unexplored fundamental science.[16, 17] The use of 2D material nanosheets as catalysts generally requires tedious exfoliation processes, which constrains mass production and industrial applications. In this regard, it is worth taking a new look at bulk materials, which have the potential to be an excellent host for a large class of species (guest) within its inner planes. An intriguing idea is that the host and intercalant can operate synergistically to achieve high efficiency and stable catalytical performance. To date, most of the intercalation methods involve ball milling of stoichiometric amounts of materials at high temperatures. The traditional approaches in chemical intercalation require electrochemical steps, limiting the concentration of intercalant.[18]

Herein, we present a facile strategy to synthesize Co^{2+} intercalated Co_9S_8 layered materials (Co^{2+}-Co_9S_8) with a layer distance of about 1.08 nm via a one-step solvothermal method. Benefiting from a large layer distance and efficient electron transfer between layers, the Co^{2+}-Co_9S_8 hybrid shows outstanding electrocatalytic hydrogen evolution performance in an acid electrolyte. The catalytical performance is even better than that of 20% Pt/C at <-0.54 V region, specifically, with an overpotential of 86 at 10 mA cm^{-2} in 0.5 mol L^{-1} H_2SO_4. More importantly, no carbon materials were

used in our system, and the intercalation of Co cations significantly enhanced the stability of Co_9S_8. This study not only presents a novel and efficient approach to synthesize Co cations intercalated cobalt sulfide for electrocatalytic HER but also provides a new avenue for the design of intercalated materials used in other energy applications.

Experimental

Chemicals and Reagents.

Cobalt nitrate hexahydrate ($Co\cdot(NO_3)_2\cdot6H_2O$, Sigma-Aldrich, ACS reagent, ≥98%), phosphorus pentasulfide (P_4S_{10}, Sigma-Aldrich, ACS reagent, 99%), ethanediamine anhydrous ($C_2H_8N_2$, Fisher scientific, ACS reagent, 99.9%), absolute ethanol (C_2H_5OH, Fisher scientific, ACS reagent, ≥99%), concentrated sulfuric acid (H_2SO_4, Fisher scientific, ACS reagent, ≥98%), and Nafion solution (Sigma-Aldrich, 5%) were used directly without any further purification. The deionized water used throughout all the experiments was purified using a Millipore system.

Synthesis of Co^{2+}-Co_9S_8.

A certain amount of cobalt nitrate (1.72 mmol, $Co(NO_3)_2\cdot6H_2O$) and phosphorus pentasulfide (0.5 mmol, P_4S_{10}) were dissolved in 70 mL ethanediamine (EDA) to form a grey solution. After stirring at room temperature for 0.5 h, the mixed solution was transferred into a 100 mL Teflon-lined autoclave, then reacted at 140 ℃ for 24 h. After the mixture cooled down to room temperature, a black product (named Co^{2+}-Co_9S_8) was obtained. The product was washed with deionized water and ethanol, then dried

under oven at 50 °C for 12 h. The intercalation amount of Co^{2+} into layered Co_9S_8 was controlled by the ratio of starting materials.

Synthesis of Co_9S_8.

The synthesis of pristine Co_9S_8 used the method reported in the literature.[19] In a typical synthesis, cobalt(II) acetate tetrahydrate (5 mmol) and thiourea (5 mmol) were dissolved in ethylene glycol (30 mL) under vigorous stirring for 30 min, then the resulting solution was transferred into an autoclave, and the autoclave was then sealed and maintained at 200 ℃ for 48 h. When the autoclave was cooled to room temperature, the samples were washed with distilled water several times to obtain pristine Co_9S_8 catalysts.

Synthesis of CoS_2.

The synthesis of CoS_2 catalysts was achieved by a previously reported method.[20] Typically, $CoCl_2 \cdot 6H_2O$ (2.5 mmol) and $Na_2S_2O_3 \cdot 5H_2O$ (2.5 mmol) were dissolved in 60 mL ultrapure water under magnetic stirring condition. Then the mixed solution was transferred into a 100 mL Teflon-lined stainless steel autoclave and subsequently agitated for another 2 h. The sealed mixture then reacted at 150 ℃ for 12 h. After the reaction, the autoclave was cooled to room temperature. The black product was harvested by filtration and washed with CS_2, ethanol, and deionized water before drying at 80 ℃ overnight.

Synthesis of $Co(OH)_2$.

The synthesis of cobalt hydroxide ($Co(OH)_2$) was reported in a previous study.[21] In detail, 4.0 mmol $CoCl_2$ (anhydrous) and 2 mmol urea were firstly dispensed in 80 mL

pure water. After stirred 2 h at room temperature, the mixture was transferred into a 100 mL Teflon-lined stainless steel autoclave, and subsequently reacted at 150 ℃ for 12 h. After the reaction, the autoclave was cooled to room temperature. The black product was harvested by filtration and washed with ethanol and deionized water before drying at 80 ℃ overnight.

Electrochemical Measurements.

All the electrochemical measurements were carried out on a SP-150 electrochemical workstation (EC-Lab, Germany) with a standard three-electrode setup (saturated calomel electrode (SCE) as the reference electrode and 1 cm^2 platinum plate were served as the counter electrode, respectively, the as-synthesized samples as the working electrode). A carbon cloth (CC, 0.1 cm^2) is used as the support for the working electrode. In detail, 4.5 mg of the samples and 20 μL Nafion solution (5 wt%) were dispersed in 1.5 mL pure water and 100 μL ethanol, and then sonicated for 30 min to form a solution. Then, 20 μL of the ink was loaded onto the surface of CC and dried at room temperature to obtain the working electrode (~0.56 $mg \cdot cm^{-2}$). The HER performances were evaluated in Ar-saturated 0.5 mol L^{-1} H_2SO_4. The electrocatalytic activity of the samples was examined by obtaining polarization curves using linear sweep voltammetry (LSV) with a scan rate of 10 $mV \cdot s^{-1}$ at room temperature. Electrochemical impedance spectroscopy (EIS) measurements were performed at different potentials from 10^5 to 10^{-2} Hz. EIS data were analyzed and fitted with the software of Zsimpwin. The stability measurements were performed by cyclic voltammetry scanning 2000 cycles (CV, sweep rate, 100 $mV \cdot s^{-1}$) and long-term chronoamperometry. Note that the

values of current density are all normalized with the geometric surface area and corrected by the background currents. All tested values in our experiments were converted to reverse hydrogen electrode (RHE) by Eq. (1)

$$E_{RHE} = E_{SCE} + 0.059\ pH + E^0_{SCE}\ (E^0_{SCE} = 0.242\ V) \quad (1)$$

Characterization.

The X-ray diffraction (XRD) patterns were collected on a Rigaku X-ray diffractometer using Cu Kα radiation (λ = 0.154 nm) at a 2θ scan rate of $0.5^o\ s^{-1}$. The accelerating voltage and applied current adopted 40 kV and 80 mA, respectively. The high-resolution transmission electron microscopy (HRTEM) and transmission electron microscopy (TEM) analysis were conducted on Tecnai G2 F20 transmission electron microscope with a 200 kV accelerating voltage. Scanning electron microscopy (SEM) images were acquired on a TESCAN LYRA3 at the accelerating voltage of 5.0 or 10 kV. Energy Dispersive X-ray spectroscopy (EDS) microanalysis was performed on a Noran system 7 by Thermo Scientific using an acceleration voltage of 20 kV. X-ray photoelectron spectroscopy (XPS) measurements were performed on an ESCALAB 250Xi electron spectrometer with Mg Kα (1253.6 eV) source. All binding energies were referenced to the C 1s peaks at 284.8 eV from the adventitious carbon. The content of Co elements in the as-prepared samples was analyzed by an inductively coupled plasma-atomic emission spectrometer (ICP-AES) on PerkinElmer Optima 7300DV. The Fourier transform infrared (FT-IR) spectra ranging from 4000 to 400 cm^{-1} were recorded by averaging 32 scans with a resolution of 4 cm^{-1} on a Thermo Nicolet 6700 FT-IR spectrometer equipped with a mercury cadmium telluride (MCT) detector. The

thickness of catalysts was executed on an atomic force microscope (AFM) with a type of Dimension 3100.

Theoretical Calculation.

In this work, all calculations were conducted with Quantum Espresso Package module based on density functional theory methods (DFT).[22-24] The form of the Perdew-Burke-Ernzerhof, PBE, functional at the generalized gradient approximation, GGA, level was employed as the exchange-correlation functional.[25-27] A plane wave basis set were used to describe electron wave functions with the cut-off energy of 550 eV. The irreducible brillouin zone was sampled by Monkhorst-Pack kpoint meshes of $2 \times 2 \times 1$ during geometry optimization and electronic properties calculations.[28] The lattice parameters, and the positions of atoms were relaxed until the maximum force, the maximum stress, the maximum displacement, maximal energy change and the self-consistent field tolerance were less than 1×10^{-8} eV/$atom$. Monolayer of Co_9S_8 crystal was constructed by cutting the bulk crystal structure along the (002) plane. The cell consisting of nine cobalt atoms and eight sulfur atoms was used as a slab model in this study. Additionally, the vacuum space was created with the set parameter of 10.8 Å along Z direction to manifest the experimental conditions. Next, the slab model of the monolayer Co_9S_8 was optimized, and the following parameters have been obtained: a = 9.927 Å, b = 9.927 Å, c = 10.800 Å, $\alpha = \beta = \gamma = 90°$. Based on the slab model computational results the Gibbs free energy, DG, has been calculated applying the formula $\Delta G = \Delta E + 0.24$ eV as proposed by Peng at al.[29] ΔE of reaction was calculated as Ecomplex-H_2-Ecomplex-HH. For the complex with Co^{2+}, binding energy of Co^{2+}-

H_2 complex has been subtracted from the final ΔE to consider two independent molecules instead of Co^{2+}-H_2 complex.

$$\Delta G = (\Delta E_{complex\text{-}H2} - \Delta E_{complex\text{-}HH} - \Delta E_{bindingH2}) + 0.24 \quad (2)$$

Results and discussion

Synthesis and Characterizations of Co^{2+}-Co_9S_8

The Co^{2+}-Co_9S_8 catalysts were prepared by a one-step solvothermal method that used cobalt nitrate and phosphorus pentasulfide as starting materials and EDA as solvent (see experiment section for the detail process). The schematic illustration of the synthesis is shown in Figure 1a. The as-prepared products were first characterized by X-ray diffraction (XRD) (Figure 1b). As a comparison, the XRD analysis of CoS_2, pristine Co_9S_8, and $Co(OH)_2$ was also carried out. In pristine Co_9S_8 pattern of Figure 1b, the peaks at 15.5°, 17.8°, 29.8°, 39.7°, 47.9°, and 52.2° can be identified as the (111), (200), (311), (331), (511) and (440) planes of the cubic Co_9S_8 phase (PDF#86-2273), respectively.[19] However, in Co cations intercalated Co_9S_8 samples, we only observed the characteristic peaks of (111), (200), (311), and (331) facets as indicated by black dots. The high index diffraction peaks of (511) and (440) disappeared. Furthermore, the crystallinity of Co_9S_8 after intercalated Co cations shows an obvious decrease compared to that of pristine Co_9S_8 (Figure S1). All these results can be attributed to some disorder within its ab plane owing to the intercalation of Co cations.[30, 31]

As solid evidence, two new peaks are observed in small-angle (8.18° and 16.36°) of XRD for Co^{2+}-Co_9S_8 samples, suggesting a long-range order layered structure of Co^{2+}-Co_9S_8. The layer distance of Co^{2+}-Co_9S_8 is further calculated based on the Bragg

equation. The result suggests that the as-obtained Co^{2+}-Co_9S_8 samples showed an expanded layer distance of 1.08 nm. The layered structure was directly observed from the HRTEM, and layer distance is in accordance with interlayer spacing measured in the edge area of HRTEM (Figure S2a). In addition, an obvious shift of (311) peaks after the intercalation of Co cations suggests that the intercalated Co cations had interaction with Co_9S_8 layers.[32]

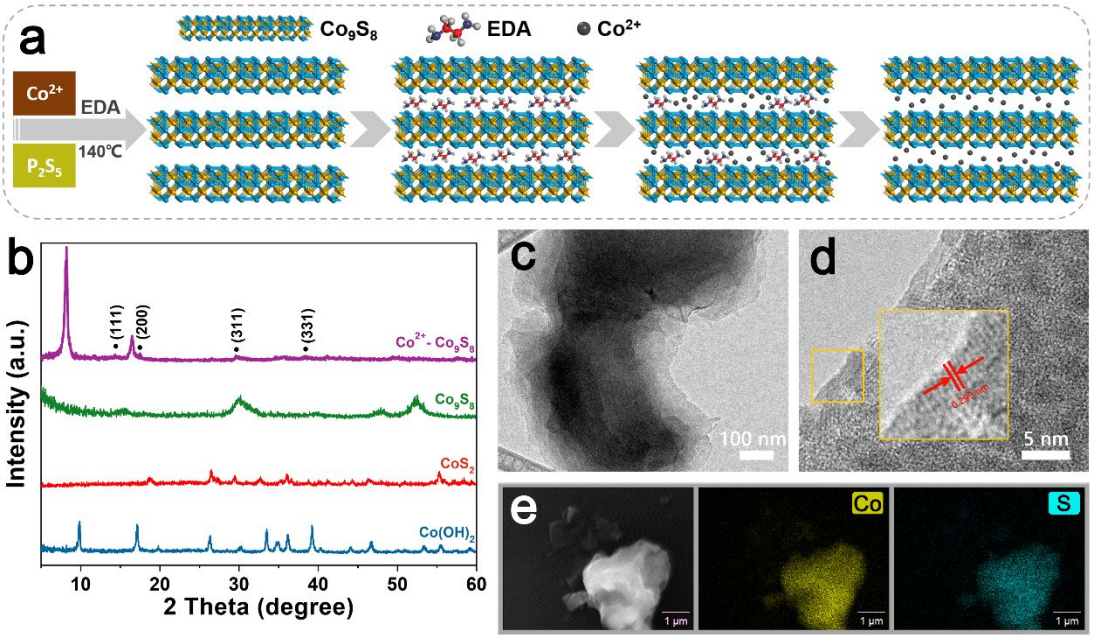

Figure 1. (a) Schematic illustration for the synthesis of Co^{2+} intercalated Co_9S_8. (b) XRD patterns of $Co(OH)_2$, CoS_2, pristine Co_9S_8, and Co cations intercalated Co_9S_8. The black dots indicate diffraction peaks corresponding to Co_9S_8 phase. (c) TEM and (d) HRTEM images of Co^{2+}-Co_9S_8. (e) SEM EDS elemental mapping of Co^{2+}-Co_9S_8.

In order to observe the layered structure of Co^{2+}-Co_9S_8, the transmission electron microscopy (TEM) and scanning electron microscopy (SEM) of samples were carried out. As presented in Figure 1c, the typical TEM image exhibits a layered structure with

a size of ~600 nm. A closer inspection of Co^{2+}-Co_9S_8 shows a lattice spacing of 0.299 nm at the edge of Co^{2+}-Co_9S_8 sample, which can be assigned to the (311) plane of Co_9S_8 (Figure 1d), indicating poor crystallinity which is consistent with the result of XRD.[33] This is consistent with the result of TEM selected area electron diffraction (Figure S3). From the cross-section of Co^{2+}-Co_9S_8 samples, an obvious layered structure was presented in Figure S4a.

To illustrate the elemental composition and distribution in Co^{2+}-Co_9S_8 samples, SEM elemental mapping was performed. As shown in Figure 1e, the two main elements of Co and S were observed in Co^{2+}-Co_9S_8 samples, and no phosphor (P) elemental signal was detected. As we expected, the amount of Co element is higher than that of S elements in Co^{2+}-Co_9S_8 samples based on SEM elemental analysis (Figure S4b and c). More importantly, the Co and S elements disperse evenly throughout the samples, and the distribution of S and Co elements overlaps. Fourier transform infrared (FT-IR) (Figure S5) results show the same peak center at 1045 cm^{-1} in Co^{2+}-Co_9S_8, CoS_2, and Co_9S_8 curves, which can be attributed to the vibration of Co-S bond. Furthermore, we have obtained the Raman spectrum of prepared Co^{2+}-Co_9S_8. As shown in Figure S6, the spectrum of Co^{2+}-Co_9S_8 sample shows the typical Raman peaks of Co_9S_8, which further confirm the formation of Co_9S_8 phase in Co^{2+}-Co_9S_8 sample.[34] Furthermore, the Raman spectra of Co^{2+}-Co_9S_8 in a range of 100-2500 cm^{-1} shows no obvious peaks, which indicates carbonization of EDA was not occur under solvothermal process. Combination with the XRD, we can conclude that these superfluous Co cations intercalated into layered Co_9S_8, and resulted in structure disorder within its ab plane,

and poor crystallinity, subsequently. Moreover, the atomic force microscope (AFM) was performed to detect the thickness of as-obtained Co^{2+}-Co_9S_8 samples. As shown in Figure S7, the thickness of the layered Co_9S_8 is ~73.0 nm, which is about ~ 68 layers based on the layer distance and the thickness of a single layer.[35]

X-ray photoelectron spectroscopy (XPS) was then carried out to identify the elemental chemical state in Co^{2+}-Co_9S_8 samples. As a control, the chemical state of pristine Co_9S_8 was also studied using C *1s* (284.8 eV) as the reference. The XPS survey spectrum (Figure S8) shows the main existence of Co and S elements and the absence of an obvious peak of P *2p* spectra (Figure S9), which is consistent with SEM elemental map study. The high-resolution XPS spectrum of Co *2p* in Co_9S_8 samples (Figure 2a) shows three peaks at Co $2p_{3/2}$ (777.7, 780.6, and 785.6 eV), and the Co $2p_{1/2}$ peak is also deconvoluted into three components with binding energies at 793.0, 796.7, and 802.1 eV. The peaks of 777.7 and 793.0 eV can be attributed to the $2p_{3/2}$ and $2p_{1/2}$ core levels of Co^{3+}, whereas the peaks centered at 780.6 and 796.7 eV are assigned to the $2p_{3/2}$ and $2p_{1/2}$ core levels of Co^{2+}, respectively. The peaks at 785.6 and 802.1 eV are the shake-up satellite peaks of Co elements.[19] As we expected, in addition to Co^{2+} and Co^{3+} of Co_9S_8, we also detected the binding energy centered at 779.1 eV for Co *2p* in the high-resolution spectrum of Co^{2+}-Co_9S_8. This binding energy can be attributed to intercalated Co^{2+} (i-Co^{2+}).[36, 37] Combining the XRD and SEM results, we conclude that partial Co cations were successfully intercalated into and had an interaction with Co_9S_8 interlayers.

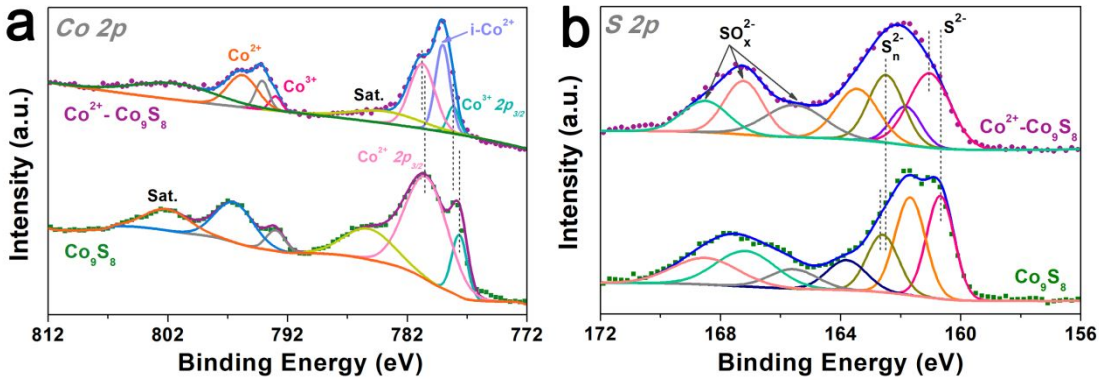

Figure 2. The high-resolution XPS spectra of (a) Co 2p and (b) S 2p in pristine Co_9S_8 and Co^{2+}-Co_9S_8 samples.

Figure 2b shows the high-resolution spectra of S *2p* for Co_9S_8 and Co^{2+}-Co_9S_8 catalysts. In pristine Co_9S_8, the binding energy at 160.7 and 162.7 eV can be attributed to the S $2p_{3/2}$ of S^{2-} and S_n^{2-} in Co_9S_8.[38] The peaks of 161.7 and 163.9 eV are assigned to corresponding $2p_{1/2}$ core levels of S *2p*. The binding energy centered at 165.6, 167.3 and 168.5 eV are due to the oxidation state of S. In the spectrum of Co^{2+}-Co_9S_8, the same chemical state of S^{2-} and S_n^{2-} were detected, confirming the formation of Co_9S_8 in Co^{2+}-Co_9S_8. The binding energy shifts were also observed in Co *2p* and S *2p* spectra in Co^{2+}-Co_9S_8 catalysts. In particular, after the intercalation of Co (II) ions into Co_9S_8, the Co element manifests higher binding energy and the S element exhibits lower binding energy. These shifts can be caused by the interaction between intercalated Co(II) ions and Co_9S_8 layers, thus resulting in the charge redistribution in Co_9S_8 layers.[39]

Based on the above analysis, we proposed a reasonable formation process of Co_9S_8 intercalated with Co cations as illustrated in Figure 1a. Bulk Co_9S_8 was firstly formed at a mild condition when using cobalt nitrate, phosphorus pentasulfide, and EDA as starting materials. In general, it is difficult for metal ions to enter into interlayers due to

the strong van der Waals forces between layers; however, it has been reported that some mechanical methods and organic solvents can effectively overcome van der Waals forces to achieve the purpose of exfoliation.[40, 41] In particular, EDA is an effective organic solvent to open layers of g-C_3N_4 under high temperatures and pressures.[42] In our system, we reason that the EDA plays a similar role in enlarging the Co_9S_8 layer distance. The organic solvent of EDA first enters into interlayers of Co_9S_8 at high temperatures and pressures and expands the layer distance of Co_9S_8. Then, through the interaction of Coulomb forces, partial cobalt ions enter into interlayers and react with layers through a surface charge to form Co_9S_8 intermediate species intercalated with Co cations and EDA. After water washing, the EDA in the interlayer was swilled out, and stable Co cations intercalated Co_9S_8 samples were formed.

Electrocatalytic performance of Co^{2+}-Co_9S_8

To evaluate the electrocatalytic HER activity of as-synthesized catalysts, a standard three-electrode electrochemical apparatus was constructed by using 0.5 mol L^{-1} H_2SO_4 as an electrolyte. Bare CC and 20%Pt/C were also tested as the reference under identical conditions. As shown in the linear sweep voltammetry (LSV) curves (Figure 3a), the Co^{2+}-Co_9S_8 hybrid requires an overpotential of 86 mV to achieve a current density of 10 mA cm^{-2}, which prominently outperforms $Co(OH)_2$ (501 mV), CoS_2 (281 mV), and Co_9S_8 (148 mV). The value is closer to an overpotential of 41 mV for 20%Pt/C. This result suggests that the intercalated Co cations play a significant role in enhancing the HER activity of Co_9S_8. Moreover, the anodic current density of the

Co^{2+}-Co_9S_8 composite surpasses that of 20%Pt/C when the applied overpotential exceeds -540 mV, highlighting the advantage of the fabricated hybrid electrode in facilitating a faster hydrogen evolution rate for large-scale applications. By plotting overpotential (η) against log current (log J), the kinetic parameters of HER were calculated. The linear part of Tafel plots (Figure 3b) reveals Tafel slopes of ~594.8, ~263.2, ~212.0, and ~30.8 mV dec^{-1} for $Co(OH)_2$, CoS_2, Co_9S_8, and 20%Pt/C, respectively. In contrast, Co^{2+}-Co_9S_8 gives a smaller Tafel slope of 115.9 mV dec^{-1} than that of pristine Co_9S_8 and even smaller than that of the reported advanced systems (Table S1), demonstrating faster HER kinetics after intercalated Co cations. The HER process likely undergoes the Volmer-Heyrovsky mechanism on the Co^{2+}-Co_9S_8 hybrid, which accelerates the water dissociation and hydrogen adsorption rates, thereby leading to an enhanced HER activity.[43]

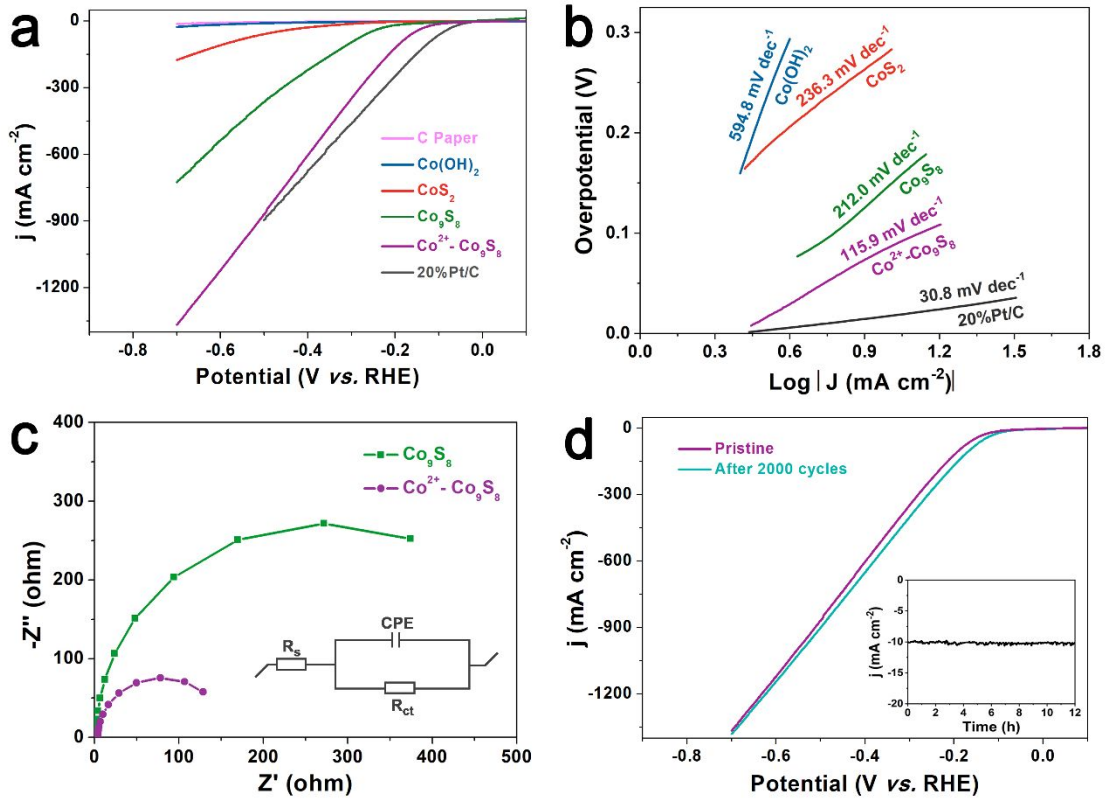

Figure 3. The electrochemical hydrogen evolution performance in 0.5 mol L^{-1} H_2SO_4 electrolyte. (a) The polarization curves of $Co(OH)_2$, CoS_2, pristine Co_9S_8, and Co^{2+}-Co_9S_8 catalysts (20%Pt/C and C paper as comparisons), the scan rate is 10 mV s^{-1}. (b) The Tafel plots of $Co(OH)_2$, CoS_2, pristine Co_9S_8, Co^{2+}-Co_9S_8, and 20%Pt/C. (c) The Nyquist plots of pristine Co_9S_8 and Co^{2+}-Co_9S_8 samples. (d) Polarization curves of Co^{2+}-Co_9S_8 catalyst at a scan rate of 10 mV s^{-1} after CV cycles for stability test. The inset is potentiostatic electrolysis of Co^{2+}-Co_9S_8 for 12 h (The potential we applied is -97 mV vs RHE). Note that the values of current density are all normalized with the geometric surface area and corrected by the background currents.

To explore the charge-transfer properties and the role of intercalated Co cations during the HER process, electrochemical impedance spectroscopy (EIS) experiments were undertaken. The semidiameter value of the Co^{2+}-Co_9S_8 system is much smaller than that of pristine Co_9S_8 (Figure 3c), implying that a smaller electron transfer resistance was achieved for Co^{2+}-Co_9S_8. Furthermore, we give corresponding relevant equivalent circuits. As shown in Figure 3c, the inset shows the equivalent circuit model used to fit the experimental data. It can be seen that all the plots exhibit a quasi-semicircle in the high-frequency region. The charge-transfer resistance R_{ct} of Co^{2+}-Co_9S_8 and pristine Co_9S_8 electrodes are 151, and 543 Ω, respectively. The lower resistance of Co^{2+}-Co_9S_8 electrode may be attributed to the effective electron transfer between Co_9S_8 layers. This further confirms that the intercalated Co cations can effectively promote the electron transfer between Co_9S_8 layers.[44] In addition, We synthesized different Co^{2+}-Co_9S_8 samples with different amounts of Co cations intercalation. As shown in Figure S10a, it exhibits the layer distance of Co_9S_8 increased with the intercalated Co amount increasing from 1.05 to 1.08 and then 1.10 nm. Furthermore, we tested the

electrocatalytic HER activity in acid solution of different Co_9S_8 samples with different layer spacing. In Figure S10b, it shows the HER activity first increased and then decreased with the increasing of layer distance. This phenomenon can be attributed to the reason described as follow. First, when the layer distance is smaller than 1.08 nm, there are abundant active sites and more effective charge transfer between Co_9S_8 intralayer, and thus leading to higher HER activity. However, further increased the layer distance of Co_9S_8 would bring poor charge transfer between layers although it still maintained abundant active sites, and thus led to the decrease of HER activity.[45, 46]

In addition to high activity, long-term catalytic durability is also very critical in practical applications. After sweeping for 2000 CV cycles between 1.3 and -0.7 V (*vs.* RHE) at 100 mV s^{-1}, the Co^{2+}-Co_9S_8 electrode almost maintains its original activity (Figure 3d), proving the salient catalytic stability. The stability is also indicated by the chronoamperometric response that displays an imperceptible decay in the overpotential at 10 mA cm^{-2} after a continuous polarization period of 12 h (inset in Figure 3d). To further confirm the stability of prepared Co^{2+}-Co_9S_8 catalysts for electrocatalytic HER, the Raman and XPS spectra of Co^{2+}-Co_9S_8 after reaction were carried out. As shown in Figure S11, the Raman spectra of Co^{2+}-Co_9S_8 sample after 12 h reaction shows unobvious change; however, the peak center at 667 cm^{-1} shows a slight shift, which may be attributed to the change of layer spacing. This may derive from the loss of intercalation Co^{2+}. Furthermore, Figure S12 shows the high-resolution spectra of Co *2p* and S *2p*. Compared to that of the sample before reaction, the XPS spectra did not show obvious change after reaction, which further suggested the excellent stability of the

prepared Co^{2+}-Co_9S_8 sample.

Mechanism study

Inspired by the remarkable HER performance, including activity and stability, of the synthesized Co^{2+}-Co_9S_8 catalysts, we further study the intrinsic mechanism of improving HER via intercalation of Co cations. The first is high HER activity. On one hand, as mentioned above, the effective electron transfer between Co_9S_8 is beneficial to improve HER activity. On the other hand, after intercalating Co cations between layers, the larger layer distance led to exposing more active sites similar to single-layer materials, and then higher HER activity.[47] To support our hypothesis, we tested BET surface area and calculated the electrochemical surface active on surface area of samples according to nitrogen adsorption-desorption isotherms and CV curves.[48] As shown in Table S2 and Figure S13, the Co^{2+}-Co_9S_8 catalyst shows an electrically active surface area of 671 mF cm^{-2}, which is much higher than that of pristine Co_9S_8 catalyst (158 mF cm^{-2}). However, the Co^{2+}-Co_9S_8 system (43.4 $m^2 \cdot g^{-1}$) exhibits a smaller BET surface area and larger pore volume than those of pristine Co_9S_8 system (55.4 $m^2 \cdot g^{-1}$). This result provides solid evidence for higher HER activity in the Co^{2+}-Co_9S_8 system via intercalation Co cations. In addition, after the intercalation of Co cations into Co_9S_8 layers, the electronic configurations and related interfacial properties of Co_9S_8 will also change and thus affect the adsorption and desorption for the hydrogen atom.[49] As shown in Table S3, after intercalation Co cations into Co_9S_8 intralayer, the value of hydrogen adsorption free energies (ΔE_H) shows an obvious decrease, which is beneficial to the desorption of formed H_2. Furthermore, to gain further insight into the underlying

mechanism of the HER catalysis, density functional theory (DFT) calculations were performed for the Gibbs free energy for hydrogen adsorption of catalysts. The adsorption Gibbs free energy of H* (ΔG_{H*}) on the catalysts serves as a parameter for the evaluation of HER activity. A large and negative value of ΔG_{H*} indicates strong chemical adsorption, while a large and positive ΔG_{H*} represents weak H* adsorption.[33] A catalyst that yields an absolute value of $\Delta G_{H*} \approx 0$ is considered a good candidate for HER, whether it is positive or negative. To further investigate the active centers, the free energy ΔG_{H*} on Co^{2+}-Co_9S_8 and pristine Co_9S_8 systems were calculated. As shown in the Gibbs free-energy diagram of Figure S14, the calculations indicated that the absolute value of ΔG_{H*} for Co^{2+}-Co_9S_8 was smaller than that of pristine Co_9S_8, and the favorable H* adsorption kinetics of the Co^{2+}-Co_9S_8 system was better than that of the pristine Co_9S_8. This was in good agreement with the electrochemical test results.

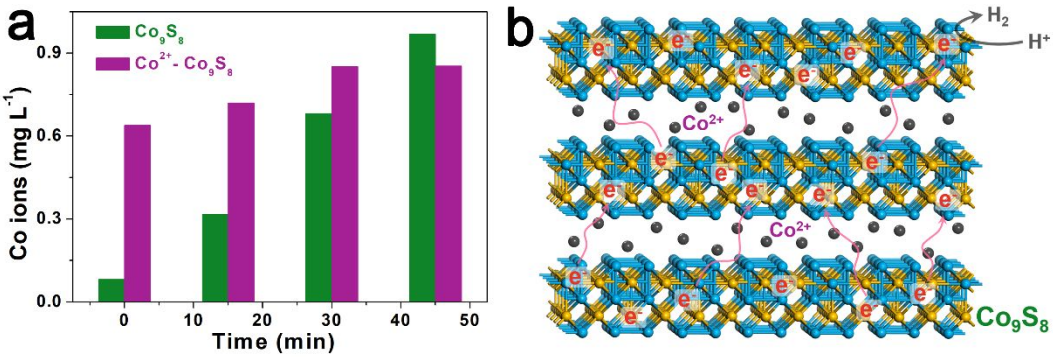

Figure 4. The concentration of Co cations in electrolyte with the electrocatalytic reaction extends from 0 to 45 min in pristine Co_9S_8 and Co cations intercalated Co_9S_8 system. (b) Schematic illustration of the electrocatalytic hydrogen evolution reaction process on Co cations intercalated Co_9S_8 catalysts.

The second is high HER stability. A previous study suggests that the high HER activity of cobalt sulfide is originated from the active sites formed on defects after dissociation of Co cations, which would lead to low stability.[50] In this regard, we

propose that the intercalated Co cations can effectively inhibit the dissociation of Co cations in Co_9S_8 and thus lead to excellent HER stability. To confirm this speculation, we detected the amount of Co cations in the electrolyte with extending reaction time. As present in Figure 4a, in the pristine Co_9S_8 system, the amount of Co cations in electrolyte shows a continuously increase with the reaction time from 0 to 45 min; however, in the Co^{2+}-Co_9S_8 system, the amount of Co cations in electrolyte shows a trend of first increasing and then staying constant. This result can be attributed to the dissociation of partially intercalated Co cations instead of Co cations in the lattice, which led to a dynamic equilibrium of Co cations between the electrolyte and Co^{2+}-Co_9S_8 electrode. As a result, excellent HER stability was achieved for the Co^{2+}-Co_9S_8 system.

Based on the above experiments and analysis, we proposed a tentative mechanism of improving electrocatalytic HER performance via the Co^{2+}-Co_9S_8 catalyst (as shown in Figure 4b). The high HER activity is mainly due to two factors: (1) more active sites caused by a large layer distance, (2) effective electron transfer between layers due to intercalated Co cations. The high HER stability is mainly originated from the effective inhibition of the dissociation of Co cations in Co_9S_8.

Conclusions

In summary, we have demonstrated that the one-step solvent method is an efficient method to synthesize Co cations intercalated Co_9S_8, and it shows significant superiority in electrocatalytic HER. The as-prepared Co^{2+}-Co_9S_8 electrode exhibits outstanding performance, including low overpotentials and faster kinetics for HER as well as

remarkable long-term catalytic durability. In particular, it shows a better HER activity than 20%Pt/C at <-0.54 V region owing to the expanded interlayer distance and efficient electron transfer between layers. Furthermore, this system shows excellent stability for more than 12 h without obvious decay because the intercalation of Co cations can effectively inhibit the dissociation of Co cations from Co_9S_8. This study not only presents a novel and efficient approach to synthesize Co cations intercalated cobalt sulfide for stable electrocatalytic HER but also provides an avenue for the design of intercalated materials used in other energy applications.

Conflict of interest

There are no conflicts to declare.

Acknowledgements

This research was supported by the National Science Foundation (grant number: HRD-1700390, DMR-2000135) and the NSF EPSCoR (grant number: OIA-1757220). We thank Dr. Losovyj for assistance with XPS experiments, Dr. Islam for electrochemical Analysis, and Dr. Pradhan for AFM measurement.

References

1. B. You and Y. Sun, *Accounts of Chemical Research*, 2018, **51**, 1571-1580.
2. I. Roger, M. A. Shipman and M. D. Symes, *Nature Reviews Chemistry*, 2017, **1**, 0003.
3. Q. Lei, R. Chen, Y. Zhao, H. Chen, X. Long, J. Tan and X. Wang, *ChemSusChem*, 2020, **13**, 3605-3613.

4. Y. Wang, B. Kong, D. Zhao, H. Wang and C. Selomulya, *Nano Today*, 2017, **15**, 26-55.
5. J. Wang, W. Cui, Q. Liu, Z. Xing, A. M. Asiri and X. Sun, *Advanced Materials*, 2016, **28**, 215-230.
6. J. Qi, W. Zhang and R. Cao, *Advanced Energy Materials*, 2018, **8**, 1701620.
7. B. Xiong, L. Chen and J. Shi, *ACS Catalysis*, 2018, **8**, 3688-3707.
8. Z. Chen, K. Leng, X. Zhao, S. Malkhandi, W. Tang, B. Tian, L. Dong, L. Zheng, M. Lin, B. S. Yeo and K. P. Loh, *Nature Communications*, 2017, **8**, 14548.
9. Z. Wu, J. Wang, K. Xia, W. Lei, X. Liu and D. Wang, *Journal of Materials Chemistry A*, 2018, **6**, 616-622.
10. S. Dou, L. Tao, J. Huo, S. Wang and L. Dai, *Energy & Environmental Science*, 2016, **9**, 1320-1326.
11. X. Zou, Y. Wu, Y. Liu, D. Liu, W. Li, L. Gu, H. Liu, P. Wang, L. Sun and Y. Zhang, *Chem*, 2018, **4**, 1139-1152.
12. X. Du, J. Huang, J. Zhang, Y. Yan, C. Wu, Y. Hu, C. Yan, T. Lei, W. Chen, C. Fan and J. Xiong, *Angewandte Chemie International Edition*, 2019, **58**, 4484-4502.
13. Q. Lu, Y. Yu, Q. Ma, B. Chen and H. Zhang, *Advanced Materials*, 2016, **28**, 1917-1933.
14. L. Wang, X. Wu, S. Guo, M. Han, Y. Zhou, Y. Sun, H. Huang, Y. Liu and Z. Kang, *Journal of Materials Chemistry A*, 2017, **5**, 2717-2723.
15. J. Yin, J. Jin, H. Lin, Z. Yin, J. Li, M. Lu, L. Guo, P. Xi, Y. Tang and C.-H. Yan, *Advanced Science*, 2020, **7**, 1903070.
16. Y. Liu, C. Xiao, P. Huang, M. Cheng and Y. Xie, *Chem*, 2018, **4**, 1263-1283.
17. K. C. Kwon, J. M. Suh, R. S. Varma, M. Shokouhimehr and H. W. Jang, *Small Methods*, 2019, **3**, 1800492.
18. K. J. Koski, C. D. Wessells, B. W. Reed, J. J. Cha, D. Kong and Y. Cui, *Journal of the American Chemical Society*, 2012, **134**, 13773-13779.
19. L.-L. Feng, M. Fan, Y. Wu, Y. Liu, G.-D. Li, H. Chen, W. Chen, D. Wang and X. Zou, *Journal of Materials Chemistry A*, 2016, **4**, 6860-6867.
20. Chen and R. Fan, *Chemistry of Materials*, 2001, **13**, 802-805.
21. Z. Sun, M. Yuan, L. Lin, H. Yang, H. Li, G. Sun, X. Yang and S. Ma, *Chemical Communications*, 2019, **55**, 9729-9732.
22. P. Giannozzi, S. Baroni, N. Bonini, M. Calandra, R. Car, C. Cavazzoni, D. Ceresoli, G. L. Chiarotti, M. Cococcioni, I. Dabo, A. Dal Corso, S. de Gironcoli, S. Fabris, G. Fratesi, R. Gebauer, U. Gerstmann, C. Gougoussis, A. Kokalj, M. Lazzeri, L. Martin-Samos, N. Marzari, F. Mauri, R. Mazzarello, S. Paolini, A. Pasquarello, L. Paulatto, C. Sbraccia, S. Scandolo, G. Sclauzero, A. P. Seitsonen, A. Smogunov, P. Umari and R. M. Wentzcovitch, *Journal of Physics: Condensed Matter*, 2009, **21**, 395502.
23. P. Giannozzi, O. Andreussi, T. Brumme, O. Bunau, M. Buongiorno Nardelli, M. Calandra, R. Car, C. Cavazzoni, D. Ceresoli, M. Cococcioni, N. Colonna, I. Carnimeo, A. Dal Corso, S. de Gironcoli, P. Delugas, R. A. DiStasio, A.

Ferretti, A. Floris, G. Fratesi, G. Fugallo, R. Gebauer, U. Gerstmann, F. Giustino, T. Gorni, J. Jia, M. Kawamura, H. Y. Ko, A. Kokalj, E. Küçükbenli, M. Lazzeri, M. Marsili, N. Marzari, F. Mauri, N. L. Nguyen, H. V. Nguyen, A. Otero-de-la-Roza, L. Paulatto, S. Poncé, D. Rocca, R. Sabatini, B. Santra, M. Schlipf, A. P. Seitsonen, A. Smogunov, I. Timrov, T. Thonhauser, P. Umari, N. Vast, X. Wu and S. Baroni, *Journal of Physics: Condensed Matter*, 2017, **29**, 465901.

24. P. Giannozzi, O. Baseggio, P. Bonfà, D. Brunato, R. Car, I. Carnimeo, C. Cavazzoni, S. de Gironcoli, P. Delugas, F. Ferrari Ruffino, A. Ferretti, N. Marzari, I. Timrov, A. Urru and S. Baroni, *The Journal of Chemical Physics*, 2020, **152**, 154105.
25. J. P. Perdew, K. Burke and M. Ernzerhof, *Physical Review Letters*, 1996, **77**, 3865-3868.
26. A. D. Becke, *Physical Review A*, 1988, **38**, 3098-3100.
27. C. Lee, W. Yang and R. G. Parr, *Physical Review B*, 1988, **37**, 785-789.
28. H. J. Monkhorst and J. D. Pack, *Physical Review B*, 1976, **13**, 5188-5192.
29. Y. Peng, B. Lu, L. Chen, N. Wang, J. E. Lu, Y. Ping and S. Chen, *Journal of Materials Chemistry A*, 2017, **5**, 18261-18269.
30. X. Zhou, B. Wilfong, H. Vivanco, J. Paglione, C. M. Brown and E. E. Rodriguez, *Journal of the American Chemical Society*, 2016, **138**, 16432-16442.
31. X. Han, K. Tao, D. Wang and L. Han, *Nanoscale*, 2018, **10**, 2735-2741.
32. B. Tian, W. Gao, X. Ning, Y. Wu and G. Lu, *Applied Catalysis B: Environmental*, 2019, **249**, 138-146.
33. Y. Liu, Z. Min, J. Jiang, K. Sun, J. Gao, Y. Shang and B. Li, *ACS Sustainable Chemistry & Engineering*, 2019, **7**, 19442-19452.
34. L.-L. Feng, G.-D. Li, Y. Liu, Y. Wu, H. Chen, Y. Wang, Y.-C. Zou, D. Wang and X. Zou, *ACS Applied Materials & Interfaces*, 2015, **7**, 980-988.
35. G. Eda, T. Fujita, H. Yamaguchi, D. Voiry, M. Chen and M. Chhowalla, *ACS Nano*, 2012, **6**, 7311-7317.
36. M. J. Thompson, K. J. Blakeney, S. D. Cady, M. D. Reichert, J. D. Pilar-Albaladejo, S. T. White and J. Vela, *Chemistry of Materials*, 2016, **28**, 1668-1677.
37. D. Zeng, Y. Qiu, S. Peng, C. Chen, J. Zeng, S. Zhang and R. Xiao, *Journal of Materials Chemistry A*, 2018, **6**, 11306-11316.
38. G. Ma, X. Xu, Z. Feng, C. Hu, Y. Zhu, X. Yang, J. Yang and Y. Qian, *Nano Research*, 2020, **13**, 802-809.
39. B. Tian, Z. Li, W. Zhen and G. Lu, *The Journal of Physical Chemistry C*, 2016, **120**, 6409-6415.
40. V. Nicolosi, M. Chhowalla, M. G. Kanatzidis, M. S. Strano and J. N. Coleman, *Science*, 2013, **340**, 1226419.
41. J. Li, J. Wang, Y. Zhang, H. Wang, G. Lin, X. Xiong, W. Zhou, H. Luo and D. Li, *2D Materials*, 2018, **5**, 021001.

42. J. Meng, Z. Lan, T. Chen, Q. Lin, H. Liu, X. Wei, Y. Lu, J. Li and Z. Zhang, *The Journal of Physical Chemistry C*, 2018, **122**, 24725-24731.
43. Y. Yang, H. Yao, Z. Yu, S. M. Islam, H. He, M. Yuan, Y. Yue, K. Xu, W. Hao, G. Sun, H. Li, S. Ma, P. Zapol and M. G. Kanatzidis, *Journal of the American Chemical Society*, 2019, **141**, 10417-10430.
44. H. Wang, X.-B. Li, L. Gao, H.-L. Wu, J. Yang, L. Cai, T.-B. Ma, C.-H. Tung, L.-Z. Wu and G. Yu, *Angewandte Chemie International Edition*, 2018, **57**, 192-197.
45. H. Lin, N. Liu, Z. Shi, Y. Guo, Y. Tang and Q. Gao, *Advanced Functional Materials*, 2016, **26**, 5590-5598.
46. D.-Y. Wang, M. Gong, H.-L. Chou, C.-J. Pan, H.-A. Chen, Y. Wu, M.-C. Lin, M. Guan, J. Yang, C.-W. Chen, Y.-L. Wang, B.-J. Hwang, C.-C. Chen and H. Dai, *Journal of the American Chemical Society*, 2015, **137**, 1587-1592.
47. Y. Wan, Z. Zhang, X. Xu, Z. Zhang, P. Li, X. Fang, K. Zhang, K. Yuan, K. Liu, G. Ran, Y. Li, Y. Ye and L. Dai, *Nano Energy*, 2018, **51**, 786-792.
48. H. Wang, Z. Lu, D. Kong, J. Sun, T. M. Hymel and Y. Cui, *ACS Nano*, 2014, **8**, 4940-4947.
49. X. Du, H. Su and X. Zhang, *ACS Sustainable Chemistry & Engineering*, 2019, **7**, 16917-16926.
50. J. Staszak-Jirkovský, Christos D. Malliakas, Pietro P. Lopes, N. Danilovic, Subrahmanyam S. Kota, K.-C. Chang, B. Genorio, D. Strmcnik, Vojislav R. Stamenkovic, M. G. Kanatzidis and N. M. Markovic, *Nature Materials*, 2016, **15**, 197-203.